doi.org/10.15407/tpwj2016.11.01

NUMERICAL ANALYSIS OF PLASMA CHARACTERISTICS OF CONSTRICTED AND FREE-BURNING ARC WITH A REFRACTORY CATHODE*

I.V. KRIVTSUN[1], **I.V. KRIKENT**[2] and **V.F. DEMCHENKO**[1]
[1]E.O. Paton Electric Welding Institute, NASU
11 Kazimir Malevich Str., 03680, Kiev, Ukraine. E-mail: office@paton.kiev.ua
[2]Dnieprodzerzhinsk State Technical University
2 Dnieprostrojevskaya Str., 51918, Dnieprodzerzhinsk, Ukraine

Self-consistent mathematical model of the processes of energy-, mass- and electric transfer in the column and anode region of the electric arc with refractory cathode was used as a basis to perform numerical analysis of thermal, electromagnetic and gas-dynamic characteristics of arc plasma for constricted (plasma) and free-burning argon arc with copper water-cooled anode. Results of calculation of characteristics of arc column plasma show that distributions of electric current density, temperature and velocity of constricted arc plasma can greatly differ from the respective distributions for free-burning arc, depending on arc current, plasmatron nozzle channel diameter and plasma gas flow rate. Characteristics of near-anode layer of plasma arc also differ significantly from the respective characteristics of free-burning arc, depending on the above arcing mode parameters. Thus, by varying arc current, plasmatron nozzle channel diameter and plasma gas flow rate, it is possible to effectively control the characteristics of thermal, electromagnetic and, particularly, dynamic impact of the constricted arc on anode metal surface. 13 Ref., 1 Table, 10 Figures.

Keywords: *constricted (plasma) arc, free-burning arc, refractory cathode, water-cooled anode, arc column, anode region, arc plasma characteristics, mathematical modeling*

Application of a constricted (plasma) arc instead of free-burning one is one of the methods to improve the effectiveness of electric arc impact on metals, and, consequently, to increase the penetration depth and nonconsumable electrode welding speed. Limitation of transverse dimensions of the column of an arc with refractory cathode by the wall of plasmatron nozzle channel can lead to an essential increase of the density of electric current and heat flow, applied by the arc to the metal being welded, and variation of plasma gas flow rate enables varying in a broad range the dynamic impact of arc plasma flow on weld pool surface. Effective practical application of plasma arc as welding heat source requires having valid information on distributed characteristics of constricted arc plasma, as well as characteristics of its thermal, electromagnetic and gas-dynamic impact on the metal being welded. As experimental determination of such, important in practical terms, plasma arc characteristics as distribution of electric current density, heat flow and gas-dynamic pressure of plasma over the weld pool surface is difficult, because of high values of arc plasma temperature and temperature of the above-mentioned surface, smallness of geometrical dimensions of the arc anode region and a number of other factors, studying the plasma arc by mathematical modeling methods seems highly relevant (see, for instance, [1–6]). Therefore, the objective of this work is detailed numerical analysis of distributed characteristics of plasma column and anode region of the constricted arc, depending on its arcing mode, as well as their comparison with the respective characteristics for a free-burning arc.

Let us consider a stationary electric arc with a refractory cathode (W) and water-cooled (non-evaporating) anode (Cu), burning in an argon flow at atmospheric pressure. We will study two variants — plasma arc, constricted by the wall of the cylindrical channel of plasmatron nozzle (Figure 1, *a*), and free-burning arc (Figure 1, *b*). At selection of mathematical model of arc plasma, we will assume that arc column plasma in both the cases is isothermal and single-component, containing only particles of shielding or plasma gas (Ar). Numerical analysis of such plasma characteristics can be performed using a self-consistent mathematical model of processes of energy-, mass-, and electric transfer in the column and anode region of the welding arc, proposed in [7], and reduced allowing for the above assumptions, as described in [8]. Assuming further that distributions of plasma character-

*Basing on the paper presented at the VIII International Conference on Mathematical Modelling and Information Technologies in Welding and Related Processes (Sept. 18–23, 2016, Odessa, Ukraine).

istics of both the constricted and free-burning arc are axisymmetric, calculation of thermal, gas-dynamic and electromagnetic characteristics can be performed in both the cases using the same system of equations, the explicit form of which in cylindrical coordinates is given in [8]. Boundary conditions for the sought functions {v, u, T, φ), where v, u are the radial and axial components of arc plasma velocity, T is its temperature, φ is the plasma electric potential, are assigned on the boundaries of calculated region $\Omega = \{0 < r < R, 0 < z < L\}$, where R is the calculated region radius, L is the length of free-burning arc/open region of the constricted arc (see Figure 1), as follows.

Conditions for velocity and temperature of plasma and electric potential on the system axis of symmetry ($r = 0$) are assigned as follows:

$$v\big|_{r=0} = 0; \ \left.\frac{\partial u}{\partial r}\right|_{r=0} = \left.\frac{\partial T}{\partial r}\right|_{r=0} = \left.\frac{\partial \varphi}{\partial r}\right|_{r=0} = 0. \qquad (1)$$

On the outer boundary of the calculated region ($r = R$), we can write for plasma velocity and electric potential [8]:

$$\left.\frac{\partial(\rho v r)}{\partial r}\right|_{r=R} = 0; \quad u\big|_{r=R} = 0; \quad \left.\frac{\partial \varphi}{\partial r}\right|_{r=R} = 0, \qquad (2)$$

where ρ is the mass density of the plasma.

We will assign boundary condition for plasma temperature at $r = R$, depending on the direction of plasma flow motion on this boundary [8]:

$$T\big|_{r=R} = T_0, \ \text{at} \ v\big|_{r=R} \le 0;$$
$$\left.\frac{\partial T}{\partial r}\right|_{r=R} = 0, \ \text{at} \ v\big|_{r=R} > 0, \qquad (3)$$

where T_0 is the ambient gas temperature.

On the boundary of arc column plasma with the anode layer which is assumed to be infinitely thin ($z = L$), we will use the condition of energy balance [7, 8], corrected allowing for the work function of anode material φ_m:

$$-\chi \left.\frac{\partial T}{\partial z}\right|_{z=L} + j_a \frac{k}{e}\left(\frac{5}{2} - \delta\right) T\big|_{z=L} = (\Delta\varphi - \varphi_m) j_a + q_a, \qquad (4)$$

where χ is the coefficient of plasma heat conductivity; $j_a = -j_z\big|_{z=L}$ is the density of electric current on the anode; k is the Boltzmann constant; e is the electron charge; δ is the constant of thermodiffusion of electrons in arc plasma; Δφ is the difference of potentials between the outer boundary of the anode layer and anode surface; q_a is the heat flow into the anode, determined according to anode region model [7], at $T_{ea} = T_a$, where T_{ea} is the electron temperature in the anode layer, $T_a = T\big|_{z=1}$ is the arc plasma temperature on its boundary with the arc column.

With good approximation, the electric potential of the anode surface can be regarded constant, and assumed, for instance, to be equal to zero. Then the boundary condition for plasma potential on the boundary of arc column with the anode layer ($z = L$) can be written as follows:

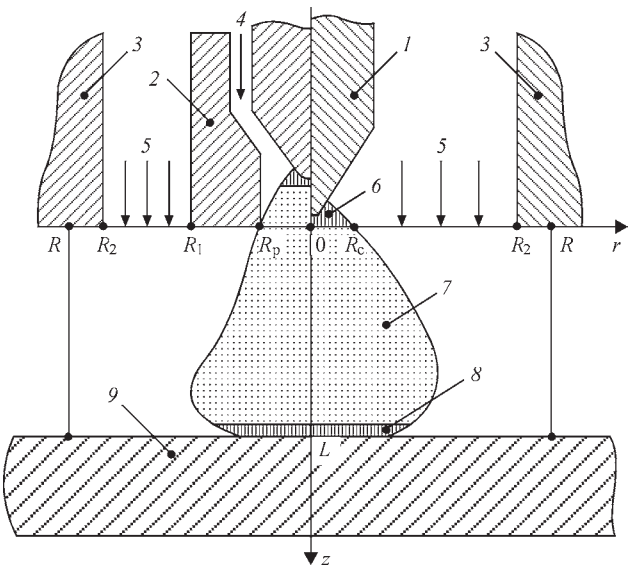

Figure 1. Schematic for calculation of characteristics of constricted (plasma) (*a*) and free-burning (*b*) arc with refractory cathode: *1* — thermocathode; *2* — plasma-forming nozzle; *3* — nozzle for shielding gas feeding; *4* — plasma gas; *5* — shielding gas; *6* — cathode region; *7* — arc column; *8* — anode layer; *9* — water-cooled anode

$$\varphi\big|_{z=L} = \Delta\varphi. \qquad (5)$$

Boundary conditions in plane $z = 0$ for free-burning arc are assigned similarly to how it was done in work [8]. In particular, in the zone of the arc cathodic binding ($r \le R_c$) (see Figure 1, *b*) the following conditions are assumed for temperature and electric potential of arc plasma:

$$T\big|_{z=0} = T_c(r); \ \ \sigma \left.\frac{\partial \varphi}{\partial z}\right|_{z=0} = j_c(r), \qquad (6)$$

where σ is the specific electric conductivity of plasma, and distributions of plasma temperature $T_c(r)$ and current density $j_c(r)$ on the boundary of cathode region with the arc column are selected by recommendations of [9].

At $R_c < R \le r$ we can write:

$$T\big|_{z=0} = T_0; \ \left.\frac{\partial \varphi}{\partial z}\right|_{z=0} = 0. \qquad (7)$$

Radial component of plasma velocity vector at $z = 0$ is taken to be zero, and conditions for axial component of velocity vector are assigned as follows:

$$u\big|_{z=0} = u_0, \ \text{at} \ r < R_2;$$
$$u\big|_{z=0} = 0, \ \text{at} \ R_2 \le r \le R, \qquad (8)$$

where u_0 is the shielding gas velocity; determined by its flow rate and inner radius of protective nozzle R_2 (see Figure 1, *b*).

As regards boundary conditions in the inlet section of the calculated region ($z = 0$) for the constricted (plasma) arc, they are assigned as follows. Assuming that the distance from the cathode working end

to plasmaforming channel edge (see Figure 1, *a*) is essentially larger than its radius R_p, it can be taken that a one-dimensional flow of arc plasma (in the direction of *OZ* axis) is in place at the channel outlet, its temperature and velocity depending only on the radial coordinate; radial components of plasma velocity and electric field intensity are equal to zero, and pressure gradient *dp/dz* and axial component of electric field E_z are constant across the channel section [1]. In this case, distributions of temperature $T(r)$ and axial component of plasma velocity $u(r)$ on the channel edge ($r \le R_p$) are found by solving one-dimensional equations:

$$\frac{1}{r}\frac{d}{dr}\left(r\chi\frac{dT}{dr}\right)+\sigma E_z^2-\psi=0; \quad (9)$$

$$\frac{1}{r}\frac{d}{dr}\left(r\eta\frac{du}{dr}\right)-\frac{dp}{dz}=0. \quad (10)$$

Here, ψ are the losses of plasma energy for radiation; η is the coefficient of plasma dynamic viscosity, and the value of axial component of electric field (electric potential gradient) $E_z = -(d\varphi/dz)$ and pressure gradient *dp*/*dz* are found from integral relationships:

$$I = 2E_z\int_0^{R_p}\sigma r dr;\ \ G = 2\pi\int_0^{R_p}\rho u r dr, \quad (11)$$

where *I* is the arc current; *G* is the mass flow of plasma gas.

Boundary conditions for equations (9), (10) are selected in keeping with the conditions of flow symmetry (1) and conditions of «sticking» on the cooled wall of plasma-forming channel that yields:

$$\left.\frac{\partial T}{\partial r}\right|_{r=0} = \left.\frac{\partial u}{\partial r}\right|_{r=0}, \quad \text{at} \quad r=0;$$
$$T = T_0; \quad u = 0, \quad \text{at} \quad r = R_p. \quad (12)$$

At $R_r < r \le R$ boundary conditions for temperature and electric potential coincide with (7), radial component of plasma velocity vector is assumed to be zero, and conditions for axial component of velocity are assigned as follows:

$$u|_{z=0} = 0, \ \text{at} \ R_p \le r \le R_1;$$
$$u|_{z=0} = u_0, \ \text{at} \ R_1 < r < R_2; \quad (13)$$
$$u|_{z=0} = 0, \ \text{at} \ R_2 \le r \le R,$$

where u_0 is the shielding gas velocity in the case of a constricted arc, determined by its flow rate, as well as inner R_1 and outer R_2 radii of the nozzle for its feeding (see Figure 1, *a*).

Initial system of equations [8], together with boundary conditions (1)–(8) for free-burning arc and (1)–(5), (9)–(13) for plasma arc, was solved numerically, by finite difference method. Temperature dependencies of thermodynamic properties, transport coefficients and emissivity of arc plasma were determined using calculated data for isothermal argon plasma of atmospheric pressure, given in [10]. At numerical solution of gas-dynamic and heat problems, joint Lagrangian–Euler method was used [11, 12], which was adapted to the conditions of the compressible medium.

Comparative numerical analysis of arc plasma characteristics, as well as characteristics of its thermal, electromagnetic and gas-dynamic impact on the anode surface for constricted (plasma) arc and free-burning arc, was performed at the following parameters: arc current I = 100, 150, 200 A; length of free-burning arc/length of plasma arc open region L = = 3 mm; diameter of plasmatron nozzle channel d = = $2R_p$ = 2, 3, 4 mm; mass flow of plasma gas (Ar) was varied in the range of $G = 0.10–0.75\cdot10^{-4}$ kg/s, that corresponds to volume flow of 0.34–2.55 l/min. In the case of plasma arc, the inner and outer radii of annular nozzle for feeding the shielding gas (Ar) R_1 = 4.4 mm, R_2 = 7.7 mm (see Figure 1, *a*); shielding gas rate u_0 = = 0.65 m/s. In the case of free-burning arc R_2 = 7.7 mm (see Figure 1, *b*); u_0 = 0.5 m/s. In both the cases, the radius of calculated region R was selected equal to 8 mm; temperature of water-cooled anode surface, temperature of plasma-forming and protective nozzle walls, as well as temperature of the fed shielding gas T_0 was taken to be equal to 500 K.

Figure 2 gives the isolines of plasma temperature in the column of constricted (see Figure 2, *a*) and free-burning arc (see Figure 2, *b*). As follows from calculated data presented in this Figure, constriction of plasma arc initial region by the wall of the channel blown by plasma gas flow, leads to a certain elongation of the isotherms along the arc axis and to increase of the length of the column high-temperature region ($T \ge$ ≥ 16000 K), compared to free-burning arc. As regards radial distributions of arc plasma temperature, in the case of 100 ampere arc, formed by a plasmatron with nozzle channel diameter of 2 mm, the temperature in the column center turns out to be somewhat higher than the respective temperature for a free-burning arc, rising insignificantly with increase of plasma gas flow (Figure 3, *a*). For the case of I = 200 A, d = 4 mm, the temperature in plasma arc center turns out to be a little lower than that for a free-burning arc (at preservation of the tendency to slight increase of axial value with G increase, shown in Figure 3, *b*), that is indicative of weakening of the effect of arc column constriction at the respective increase of current and diameter of plasmaforming channel.

A more clearly marked feature appears in calculated distributions of electric current density in the arc column, given in Figure 4. In both the considered cases current density in the center of plasma arc column turns out to be lower than the respective values for a free-burning arc (see Figure 4). An important circumstance here is the change of the nature of radial distribution of value $|j_z|$ for a constricted arc, compared with the free-burning one, namely, appearance of a «plateau» in the respective distributions near the column axis (see solid curves in Figure 4).

Figure 5 gives the results of distributions of the axial component of arc plasma velocity in the midsection of the column of the constricted and free-burning arc (z = 1.5 mm). As follows from calculated data, given in this Figure, plasma velocity in the constricted arc column is much higher than the velocity of arc plasma for a free-burning arc, rising slightly with increase of plasma arc current and plasma-forming channel diameter (see respective solid curves in Figure 5), and significantly (almost proportionally) rising at increase of plasma-forming gas flow rate (see curves *1*, *2* in Figure 5).

Before going over to analysis of near-anode plasma characteristics, it should be noted that one of the causes for the above behavioural features of radial distributions of plasma temperature and electric current density in the constricted arc column at increase of current and diameter of plasma-forming channel relative to the respective distributions for a free-burning arc, can be selection of boundary conditions for plasma temperature and velocity at the edge of plasmatron nozzle channel in the form of (9), (10). So, at small values of channel diameters use of the assumption of one-dimensionality of arc plasma flow at the channel outlet and use of conditions (9, (10), respectively, appears sufficiently substantiated, while at R_p increase more correct results can be obtained by solving the initial equations in the entire region, including that of arc plas-

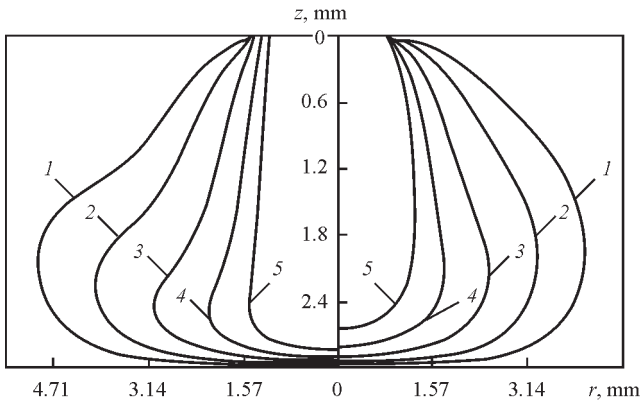

Figure 2. Isolines of temperature of column plasma in constricted (*a*) and free-burning (*b*) argon arc with a refractory cathode (W) and water-cooled anode (Cu) at current I = 150 A, arc open region length L = 3 mm, plasma-forming channel diameter d = 3 mm and plasma gas flow rate (Ar) $G = 0.4 \cdot 10^{-4}$ kg/s (1.36 l/min): *1* — T = = 10; *2* — 12; *3* — 14; *4* — 16; *5* — 18 kK

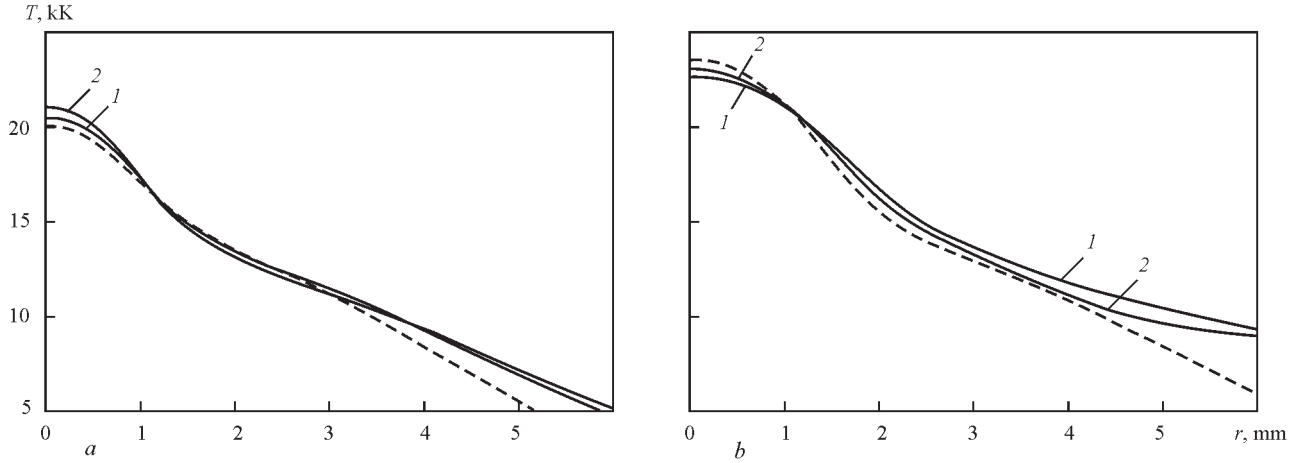

Figure 3. Radial distributions of plasma temperature in section z = 1.5 mm of plasma arc column: *a* — *1* = 100 A; d = 2 mm; *1* — $G = 0.1 \cdot 10^{-4}$ kg/s (0.34 l/min), *2* — $G = 0.2 \cdot 10^{-4}$ kg/s (0.68 l/min); *b* — *1* = 200 A; d = 4 mm; *1* — $G = 0.4 \cdot 10^{-4}$ kg/s (1.36 l/min); *2* — $G = 0.75 \cdot 10^{-4}$ kg/s (2.55 l/min) (dashed curves are the respective distributions for free-burning arc)

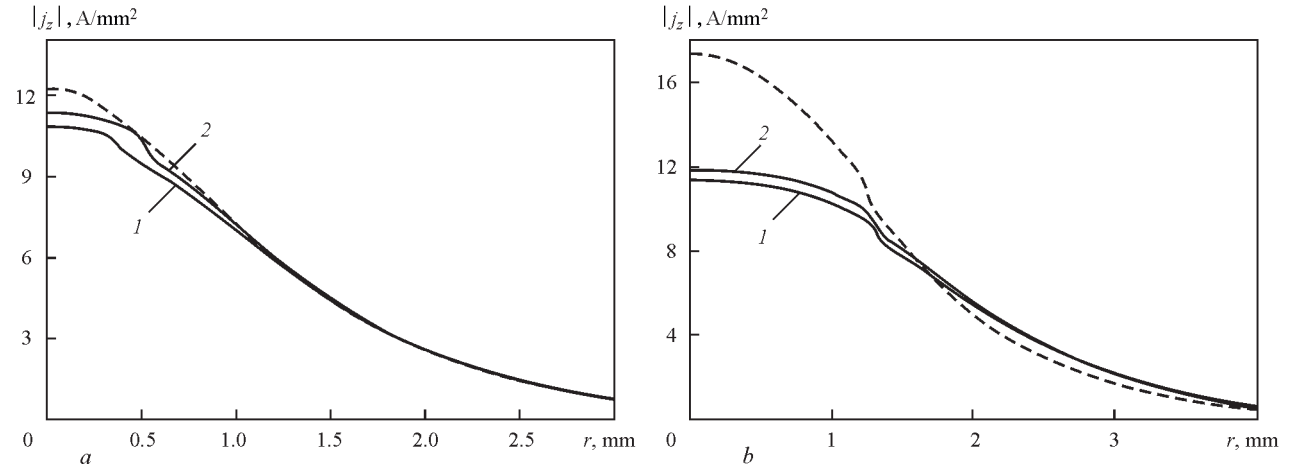

Figure 4. Radial distributions of axial component of electric current density in section z = 1.5 mm of the column of plasma and free-burning arc (parameters and designations are the same, as in Figure 3)

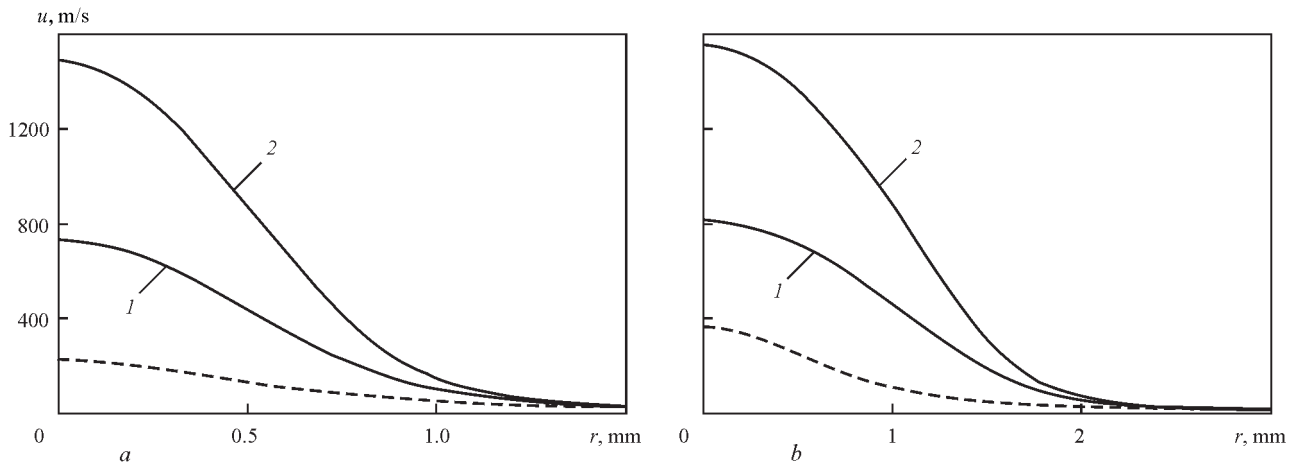

Figure 5. Radial distributions of axial component of plasma velocity in section z = 1.5 mm of the column of plasma and free-burning arc (parameters and designations are the same, as in Figure 3)

ma inside the plasmatron nozzle channel (see Figure 1, *a*), that we intend to do at the next research stage.

Figures 6, 8 give the calculated distributions of arc plasma characteristics on the boundary of the anode layer with the arc column, and Figures 7, 9, 10 show the distributed characteristics of its electric, thermal and dynamic impact on the anode surface. Unlike radial distributions of plasma temperature in the arc column (see Figure 3), arc plasma temperature near the constricted arc anode turns out to be markedly higher than the near-anode plasma temperature for a free-burning arc, increasing with the increase of plasma gas flow rate, here profile $T_a(r)$ becomes «fuller» with G rise (see Figure 6). This is related to more effective transfer of thermal energy towards the anode by high-velocity flow of constricted arc plasma, compared to a relatively weak convective transfer of thermal energy in the case of a free-burning arc (see Figure 5).

Distributions $j_a(r)$ given in Figure 7, are indicative of a higher degree of contraction of 100 A plasma arc anode region, compared to a free-burning one, while at I = 200 A the opposite is observed (see Figure 7). In addition, similar to radial distributions of near-anode plasma temperature, the profiles of electric current density distribution on plasma arc anode become «fuller» with increase of plasma gas flow, due to a certain lowering of current density on the axis (compare curves *1*, *2* in Figure 7). The cause for that are not only the above features of behaviour of $T_a(r)$ distributions for a constricted arc (see Figure 6), but also restructuring of radial distributions of plasma potential on the boundary of the column with plasma arc anode layer, compared to free-burning arc (Figure 8). As shown in [13], this leads to a change of radial component of electric field intensity $E_r = -(d\varphi/dr)$, in the considered case — to its reduction in the near-axis zone of the anode region (see Figure 8), and, consequently, to a change of the vector of electric current density in near-anode arc plasma, which determines the pattern of current flowing between the plasma and anode surface.

Figure 9 gives radial distributions of the heat flow applied by the arc to the anode. In case of 100 A plasma arc (d = 2 mm) value q_a significantly exceeds the

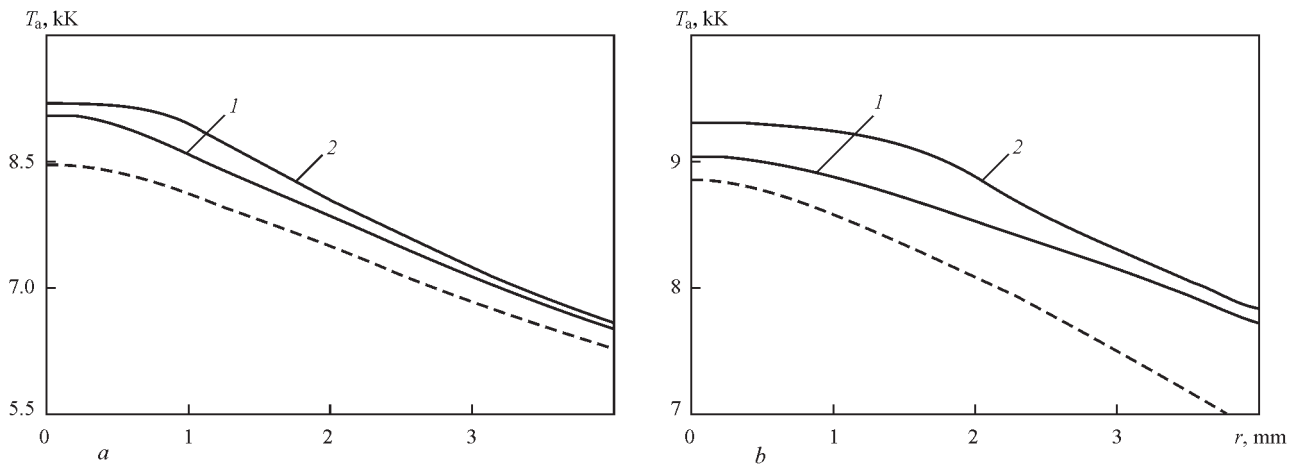

Figure 6. Radial distributions of plasma temperature on the boundary of plasma arc anode layer: *a* — I = 100 A; d = 2 mm; *1* — G = $= 0.1 \cdot 10^{-4}$ kg/s (0.34 l/min), *2* — $G = 0.2 \cdot 10^{-4}$ kg/s (0.68 l/min); *b* — I = 200 A; d = 4 mm; *1* — $G = 0.4 \cdot 10^{-4}$ kg/s (1.36 l/min), *2* — G = $= 0.75 \cdot 10^{-4}$ kg/s (2.55 l/min) (dashed curves are the respective distributions for free-burning arc)

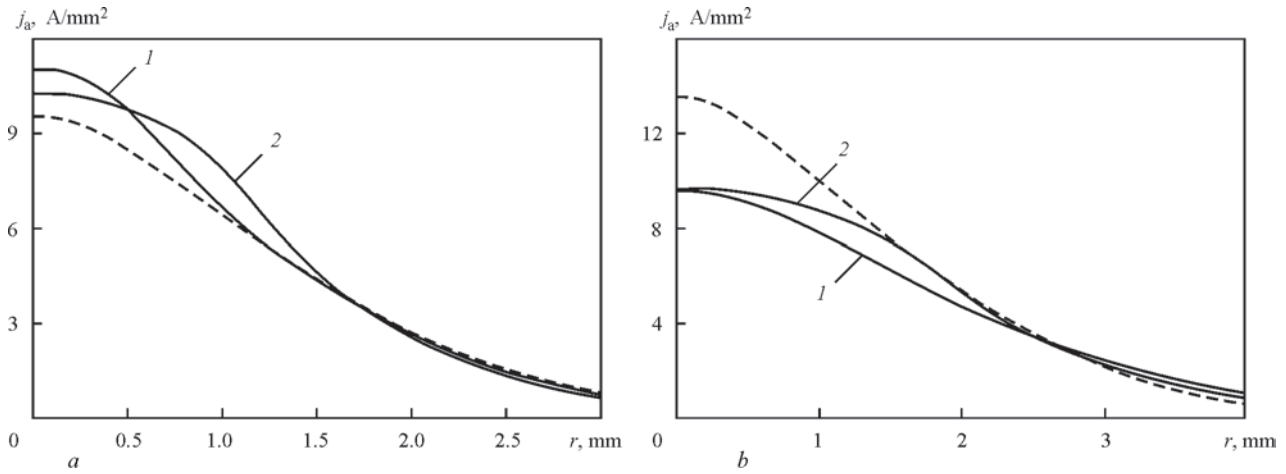

Figure 7. Radial distributions of electric current density on the anode of plasma and free-burning arc (parameters and designations are the same as in Figure 6)

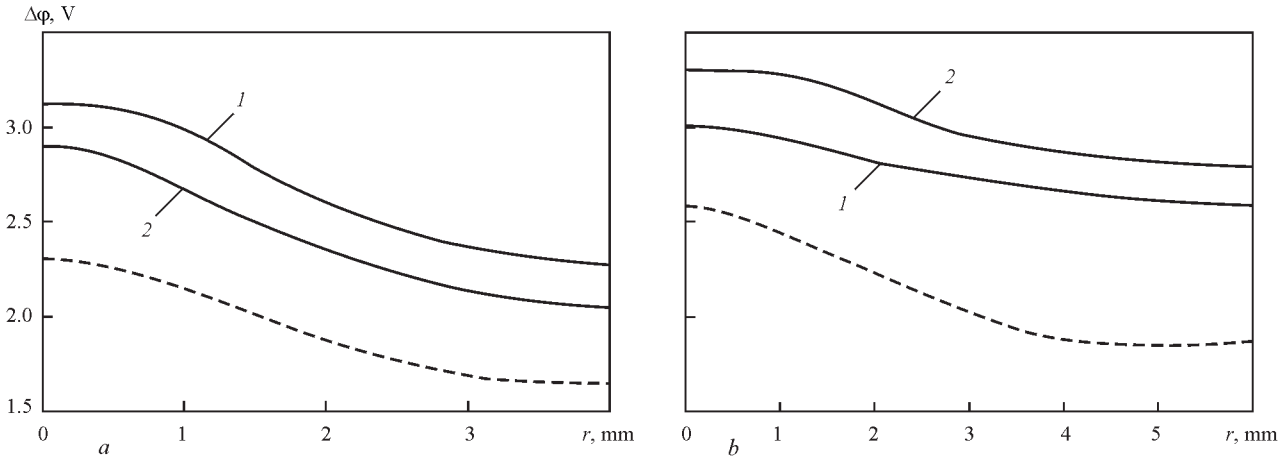

Figure 8. Radial distributions of plasma potential on the boundary of anode layer of plasma and free-burning arc (anode surface potential was taken to be constant and equal to zero, parameters and designations are the same as in Figure 6)

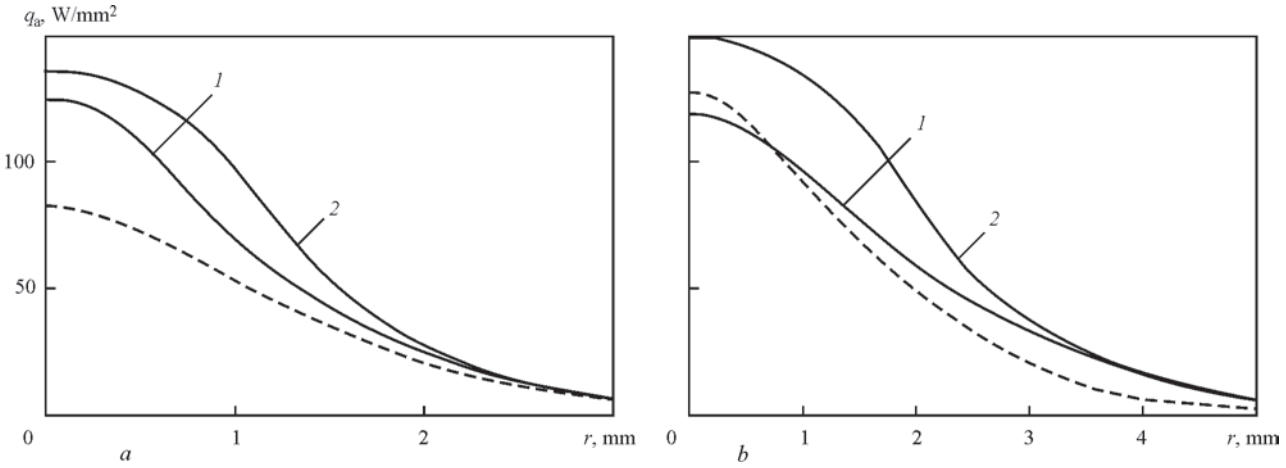

Figure 9. Radial distributions of heat flow to the anode for plasma and free-burning arc (parameters and designations are the same as in Figure 6)

respective values for a free-burning arc; and with increase of plasma gas flow rate an increase of heat flow density, disproportional by the radial coordinate is observed, leading to its profile becoming fuller (see Figure 9, *a*). At I = 200 A (d = 4 mm), axial value of heat flow applied to the anode by the constricted arc, can be both smaller than value $q_a(0)$ for a free-burning arc (at low flow rate of plasma gas), and greater than it (at G increase), as shown in Figure 9, *b*. As regards integral values of power applied by the arc to the anode $Q_a = 2\pi \int_0^\infty q_a r dr$, in all the considered cases, this value for the plasma arc turns out to be significantly

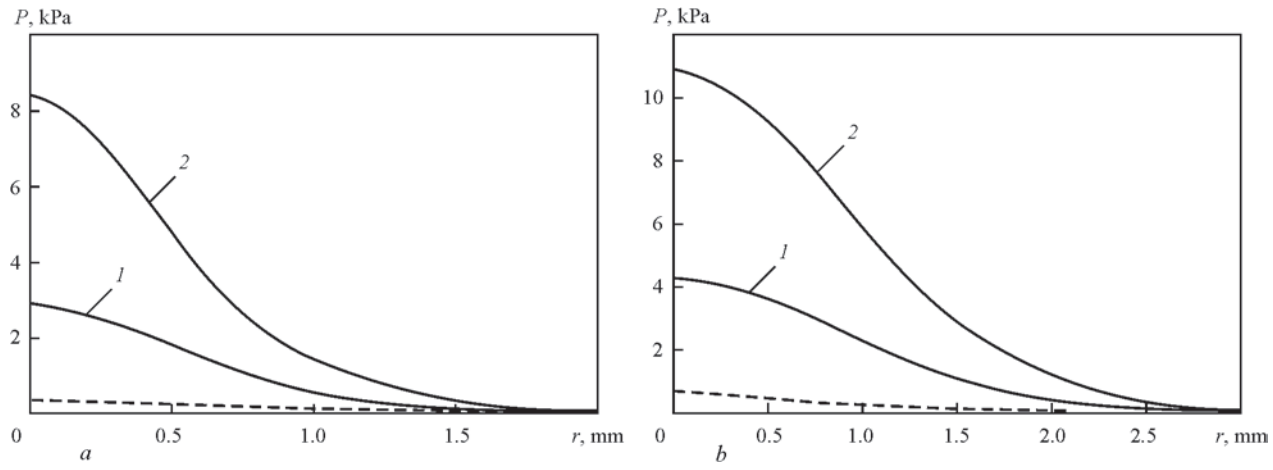

Figure 10. Radial distributions of gas-dynamic pressure of plasma flow to the anode surface for plasma and free-burning arc (parameters and designations are the same as in Figure 6)

Power Q_a applied to the anode by a constricted (plasma) arc and free-burning argon arc

Arc type	I = 100 A (d = 2 mm)	I = 200 A (d = 4 mm)
Free-burning	789 W	1724 W
Constricted (plasma)	999 W (G = 0.34 l/min)	2518 W (G = 1.36 l/min)
	1187 W (G = 0.68 l/min)	3139 W (G = 2.55 l/min)

higher than that for a free-burning one, and it rises with increase of plasma gas flow rate, as follows from calculated data given in the Table. The main cause for that is intensive transfer of thermal energy from the high-temperature region of the constricted arc column towards the anode, performed by a higher-velocity flow of arc plasma, than in the case of a free-burning arc (see Figure 5).

Another important characteristic of the arc impact on the anode surface is gas-dynamic pressure P of arc plasma flow on the above surface. Calculated distributions of value P along the anode surface are given in Figure 10. As follows from the calculated data given in this Figure, gas-dynamic pressure on the surface of constricted arc plasma anode is significantly higher than the respective values for a free-burning arc, increasing with increase of plasma arc current and plasmatron nozzle channel diameter (compare the respective solid curves in Figure 10, *a*, *b*), and rising considerably at increase of plasma gas flow rate (compare curves *1* and *2* in Figure 10, *a*, 10, *b*).

On the whole, modeling results, presented in the Table and in Figures 7, 9, 10 lead to the conclusion that change of plasma gas flow rate in plasma welding is an effective means of influencing not only the value and distribution of gas-dynamic pressure of constricted arc plasma on weld pool surface, but also the respective characteristics of its thermal and electromagnetic impact on the metal being welded.

1. Engelsht, V.S., Gurovich, V.Ts., Desyatkov, G.A. et al. (1990) *Low-temperature plasma*. Novosibirsk: Nauka. Vol. 1: Theory of electric arc column.
2. Beulens, J.J., Milojevic, D., Schram, D.C. et al. (1991) A two-dimensional nonequilibrium model of cascaded arc plasma flows. *Phys. Fluids B*, 3(**9**), 2548–2557.
3. Dowden, J., Kapadia, P. (1994) Plasma arc welding: a mathematical model of the arc. *J. of Physics D: Applied Physics*, 27(**5**), 902–910.
4. Wendelstorf, J., Decker, I., Wohlfahrt, H. et al. (1996) TIG and plasma arc modeling: a survey. Mathematical modelling of weld phenomena 3. London: *The Institute of Materials*, 848–897.
5. Jenista, J., Heberlein, V.R., Pfender, E. (1997) Numerical model of the anode region of high current electric arcs. *IEEE Transact. on Plasma Sci*., 25(**5**), 883–890.
6. Schnick, M., Fuessel, U., Spille-Kohoff, A. (2010) Numerical investigations of the influence of design parameters, gas composition and electric current in plasma arc welding (PAW). *Welding in the World*, **54**(Issue 3), 87–96.
7. Krivtsun, I.V., Demchenko, V.F., Krikent, I.V. (2010) Model of the processes of heat-, mass- and charge transfer in the anode region and column of the welding arc with refractory cathode. *The Paton Welding J*., **6**, 2–9.
8. Krikent, I.V., Krivtsun, I.V., Demchenko, V.F. (2012) Modelling of processes of heat-, mass- and electric transfer in column and anode region of arc with refractory cathode. *Ibid*., **3**, 2–6.
9. Wendelstorf, J., Simon, G., Decker, I. et al. (1997) Investigation of cathode spot behavior of atmospheric argon arcs by mathematical modeling. In: *Proc. of the 12th Int. Conf. on Gas Discharges and their Applications* (Germany, Greifswald, 1997). Vol. 1, 62–65.
10. Boulos, M.I., Fauchais, P., Pfender, E. (1997) *Thermal plasmas: Fundamentals and applications*. New York and London: Plenum Press, Vol. 1.
11. Lyashko, I.I., Demchenko, V.F., Vakulenko, S.A. (1981) Version of method of splitting of equations of viscous incompressible fluid dynamics on Lagrange–Euler lattices. *Doklady AN Ukr.SSR. Seriya A*, **7**, 43–47.
12. Demchenko, V.F., Lesnoj, A.B. (2000) Lagrange-Euler method of numerical solution of multidimensional problem of convective diffusion. *Dopovidi NANU*, **11**, 71–75.
13. Krivtsun, I.V., Krikent, I.V. Demchenko, V.F. et al. (2015) Interaction of CO_2-laser radiation beam with electric arc plasma in hybrid (laser + TIG) welding. *The Paton Welding J*., **3/4**, 6–15.

Received 04.10.2016